frontiers | Frontiers in Mechanical Engineering

TYPE Original Research
PUBLISHED 12 January 2026
DOI 10.3389/fmech.2025.1728504

OPEN ACCESS

EDITED BY
Chengxi Zhang,
Jiangnan University, China

REVIEWED BY
Florian Allein,
University of California, San Diego, United States
Yuyang Chen,
Guangzhou University, China
Peilin Jia,
Dalian University of Technology, China

*CORRESPONDENCE
Ying Wang,
18915515923@163.com

RECEIVED 20 October 2025
REVISED 17 December 2025
ACCEPTED 22 December 2025
PUBLISHED 12 January 2026

CITATION
Wang Y, Yu S, Jiang C and Hu J (2026) Valley-protected topological interface states in metastructures with internal geometric rotation. *Front. Mech. Eng.* 11:1728504.
doi: 10.3389/fmech.2025.1728504

Valley-protected topological interface states in metastructures with internal geometric rotation

Ying Wang*, Shuang Yu, Chengcan Jiang and Jing Hu

School of Intelligent Equipment, Suzhou Vocational Institute of Industrial Technology, Suzhou, China

Topological mechanical metamaterials have garnered significant attention for their ability to exhibit robust, defect-immune wave propagation and mechanical behaviors, inspired by topological protection mechanisms in condensed matter physics. In this study, we present a novel mechanical metamaterial design that introduces rotational geometric parameters within the unit cell to explicitly break spatial inversion symmetry. By precisely tuning the rotation angle of structural elements in the unit cell, we induce asymmetric valley states with opposite Berry curvatures, thereby realizing the valley Hall effect in a mechanical framework. This purely geometric approach avoids reliance on material composition gradients or external fields, offering intrinsic control over valley polarization through structural design alone. Numerical simulations and mechanical analyses demonstrate that the proposed metamaterial supports topologically protected interface states at the boundary between regions of distinct valley topologies. These interface states exhibit unidirectional propagation, confirming their topological protection. This work provides a universal geometric strategy to engineer topological phenomena in structural systems. The realized topologically protected interface states hold promise for applications in high-precision sensors, energy harvesting devices, and vibration isolation systems.

KEYWORDS

elastic wave, metamaterial, topological interface state, topological mechanical metamaterials, valley hall effect

1 Introduction

In recent decades, metamaterials have garnered extensive research attention in the fields of mechanics and physics (Li et al., 2020; Jiao et al., 2023; Ni et al., 2023; Chen C. et al., 2025; Du et al., 2025; Chen et al., 2024c; Dong et al., 2024; Akbari-Farahani and Ebrahimi-Nejad, 2024; Ni and Shi, 2023; Chen et al., 2023). This is primarily attributed to their unique capability of achieving novel mechanical properties through rational design of structural architectures, rather than relying solely on the inherent composition of base materials.

Natural materials are inherently constrained in their acoustic and elastic wave propagation characteristics, as such capabilities are fundamentally limited by their intrinsic lattice structures and continuous physical properties. In sharp contrast, artificially engineered metamaterials—crafted with high-precision design and fabrication—can markedly enhance the flexibility of manipulating and controlling acoustic and elastic waves, breaking through the inherent restrictions of natural materials.

Researchers have now developed numerous types of metamaterials exhibiting extraordinary physical properties, such as negative effective density, negative elastic modulus, and negative refractive index. These anomalous characteristics are fundamentally rooted in theoretical frameworks including local resonance (Santoro et al., 2023; Wang et al., 2025), Bragg scattering (Jia et al., 2025; Rao et al., 2024), transformation acoustics (Cao et al., 2025; Pendry et al., 2006), topological bands (Chu et al., 2024), and non-Hermitian physics (Cao et al., 2022), enabling the realization of remarkable physical phenomena including but not limited to: (1) diffraction-limited acoustic focusing, (2) broadband noise dissipation, and (3) resonant vibration isolation.

Traditional metamaterials achieve equivalent parameters such as negative refractive index and negative modulus through specific structural designs (e.g., resonant units). These properties are highly sensitive to defects and disorder—any structural damage or manufacturing deviations can cause these characteristics to significantly weaken or disappear. In other words, traditional metamaterials macroscopically mimic material parameters not found in nature, and their functionality relies on structural perfection. In contrast, the extraordinary properties of topological metamaterials originate not from the emulation of specific parameters, but rather from the global topological characteristics inherent in their structural band structures. As a result, wave propagation in topological metamaterials (such as waves at the boundaries) is globally protected. Even in the presence of internal defects, manufacturing imperfections, or sharp bends in the path, the waves can propagate along the boundary—they are not only dissipationless and unidirectional but also unaffected by these disturbances or local perturbations. Inspired by topological insulators in quantum physics (Haldane, 1988; Klitzing et al., 1980; Den, 1982), researchers have developed three major categories of topological metamaterials within classical physics domains such as acoustics and mechanics.

The first approach draws on topological insulators based on the Quantum Hall Effect (QHE) (Susstrunk and Huber, 2015). By breaking time-reversal symmetry through globally rotating the coupled pendulum array, a topologically non-trivial phase is induced. The results demonstrate that vibrational energy propagates unidirectionally along the lattice boundary with remarkable robustness—even in the presence of defects or disordered structures, the energy bypasses obstacles without backscattering and continues to propagate. A hexagonal lattice structure designed by Nash et al. incorporates gyroscopes at its nodal points (Nash et al., 2015), utilizing their rotational effects to break time-reversal symmetry, thereby enabling the development of topological metamaterials based on the Quantum Hall Effect. The second way, inspired by Bernevig and Zhang (2006), does not need to break time-reversal symmetry. The fundamental principle of this class of metamaterials is similar to the spin-orbit coupling mechanism observed in QSHE. Chen et al. (2024a) designed a Kekule lattice-based elastic topological resonator with tunable coupling strip widths using the quantum spin Hall effect, achieved robust edge state transmission through topological phase transitions, and realized frequency-space separation by integrating the topological rainbow effect—providing a novel mechanism for efficient elastic wave manipulation and the development of programmable sensors. Zhang et al. developed a groundbreaking methodology by employing a flow-free metamaterial lattice with deliberately broken structural symmetry (Zhang et al., 2017), successfully constructing acoustic pseudo-spin multipole states. Through systematic investigation, the research team demonstrated that implementing symmetry-breaking operations in a honeycomb lattice and regulating the interaction strength between resonant units within the lattice can achieve band inversion between pseudo-spin dipole and quadrupole states. This mechanism serves as a pivotal factor in driving topological phase transitions. Chen et al. (2025c) for the first time introduces topological Wannier cycles into full-polarization micromechanical metamaterials, realizes broadband robust elastic dislocation states via helical dislocation structures, enhances energy harvesting and frequency identification capabilities using mode conversion and coupling systems, and provides a new paradigm for full-polarization elastic wave manipulation. Chen et al. (2018) developed an innovative approach to realize a mechanical quantum spin Hall insulator and successfully modeled this quantum phenomenon using a simplified mass-spring Kagome lattice structure. By employing the Brillouin zone folding technique, the model constructed a lattice system featuring double Dirac cones, opening new research dimensions and methodological pathways for exploring the mechanical quantum spin Hall Effect. Chen et al. (2025b) establishes an electro-acoustic analogy model to achieve second-order to quadrupole topological transition in acoustic metamaterials, investigates multi-dimensional localized states in dislocation structures, and provides a robust framework for acoustic topological manipulation with promising applications in sensing, signal processing, and energy harvesting. Mousavi et al. (2015) proposed the design of a dual-scale phononic crystal plate featuring a triangular lattice of air holes, which achieved degenerate Dirac cones for both symmetric and antisymmetric Lamb wave modes. Subsequently, by breaking spatial mirror symmetry, strong spin-orbit coupling was introduced, leading to a topological phase transition and the formation of a complete phononic bandgap. Chen et al. (2024b) innovatively combines topological insulators with the rainbow trapping effect, designs surface wave photonic crystals based on concrete-filled steel tubes (CFST), achieves robust transmission, frequency-spatial separation, and energy concentration of low-frequency surface waves, and provides a new scheme with both theoretical value and application potential for surface wave manipulation in fields such as reconfigurable seismic metamaterials, sensing, and energy harvesting.

The third method for achieving topologically protected edge states, based on the quantum valley Hall effect (QVHE) (Dong et al., 2024; Chen et al., 2023; Liu et al., 2019), is relatively more straightforward. This approach relies solely on breaking spatial inversion symmetry. QVHE-based topological metamaterials

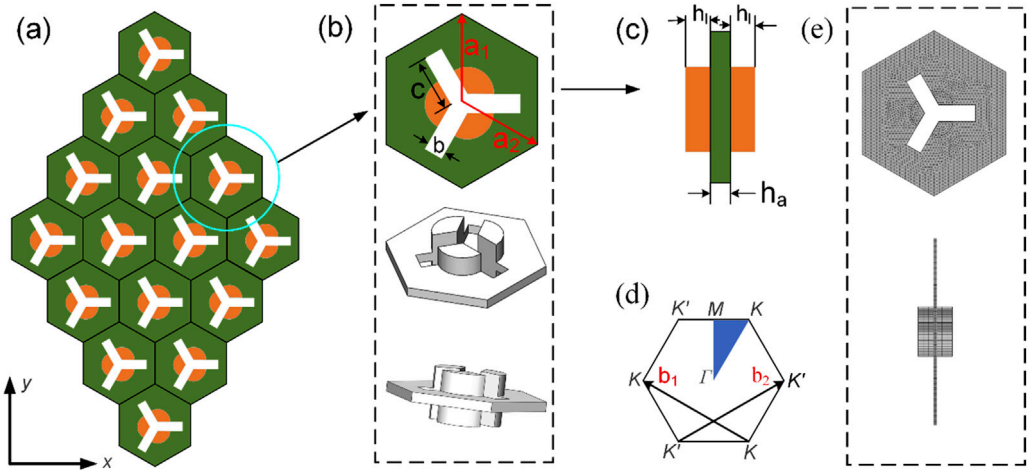

FIGURE 1
(a) Illustration of the metamaterial with lattice vector $a_1 = (a/2, \sqrt{3}a/2)$ and $a_2 = (-\frac{a}{2}, \sqrt{3}a/2)$; **(b)** unit cell structure, the green hexagons represents the thin aluminum plate, while the orange parts represent the fan-shaped structures made of lead material; **(c)** the section view of the unit cell, the heights of the aluminum hexagonal thin plate and the lead fan-shaped structure are h_a and h_l, respectively; **(d)** The Brillouin zone of the unit cell; **(e)** The mesh distribution in the unit cell, the minimum element in the unit cell is 0.012 mm, the maximum element is 1.2 mm, and the model adopts Quadratic serendipity and triangular prism elements.

preserve time-reversal symmetry, simplifying geometric complexity. Lu et al. (2016) developed a novel mechanism for breaking mirror symmetry, successfully constructing an acoustic analogue of the topological semimetal-insulator phase transition. By precisely adjusting the rotation angles of anisotropic scatterers within the phononic crystal, it is able to control the shape of the frequency bandgap and phase domain walls. Li et al. (2019) put forward a creative design framework for elastic metamaterials, termed "valley anisotropy," which can be achieved via an asymmetric structural scheme integrating bio-inspired hard helical scatterers and a compliant material matrix. The research team verified that Berry curvature—a crucial topological indicator—can be accurately regulated by modifying the geometric parameters. This regulation mechanism enables the topological manipulation of transverse elastic waves, thereby allowing for the control of energy propagation behaviors, including the redirection and termination of energy flow. Zhang et al. (2022) present a valley phononic crystal, which consists of a hexagonal aluminum plate equipped with six support rods arranged in a chiral configuration. By tuning the lengths of these support rods within the chiral unit cell, a novel complete bandgap is induced at the Dirac point, and this bandgap formation is accompanied by the appearance of topological edge modes. The authors analyzed the dispersion characteristics of the chiral system and applied them to interface waveguides, thereby enabling the implementation of customizable propagation path designs. In addition, the team also provides evidence for the existence of the valley Hall effect in the proposed chiral system.

The programmable metamaterials have been proposed for the manipulation of elastic and electromagnetic waves (Qi et al., 2022; Xiu et al., 2022; On et al., 2024; Abadal et al., 2020; Yi et al., 2023; Darabi et al., 2020; Zhang et al., 2019). Darabi et al. (2020) proposed breaking time-reversal symmetry through time modulation, inducing synthetic angular momentum bias and opening a topological bandgap with protected edge states. The reconfigurable topological metamaterials enable robust acoustic wave transmission and are applicable to devices such as acoustic emitters and mechanical logic circuits. These systems outperform their electronic counterparts under harsh operating conditions. Zhang et al. (2019) innovatively proposed using programmable ferrofluid distributions within the unit cells of elastic lattices to break inversion symmetry and create tunable bandgaps. This approach allows for easy reconfiguration of propagation paths by controlling the ferrofluid distribution. Numerical simulations and experimental tests demonstrate the ability to guide bending waves along different interface paths, highlighting the potential applications of this programmable elastic valley-Hall insulator.

By introducing a difference in elastic stiffness, the Dirac cone can be opened, resulting in the formation of a topologically nontrivial bandgap. With the assistance of a programmable external electric field, the elastic stiffness distribution within each unit cell can be independently modified. This allows for the creation of topologically protected interface paths with arbitrary, programmable shapes in the elastic lattice, leveraging the valley degrees of freedom. Then, the distinct localized interface state is discussed. Finally, the paper discusses the application of programmable topological interface states in the domain of haptic feedback.

2 Model and theory

2.1 Topological structures

As shown in Figure 1c, the proposed model consists of periodically arranged hexagonal unit cell. Each unit cell consists

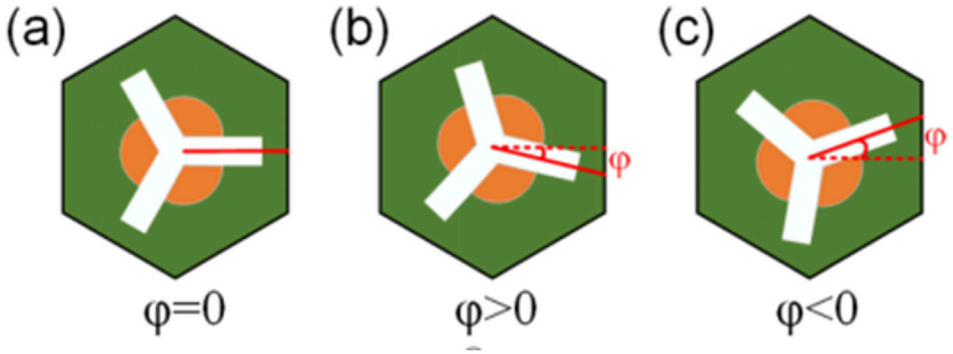

FIGURE 2
Illustration of the unit cell structure with **(a)** φ = 0, **(b)** φ > 0 and **(c)** φ < 0.

of two parts as seen in Figure 1b. One part is the Aluminum hexagonal thin plate as shown in the green part of the picture. The other part consists of three raised fan-shaped structures made of Lead material, which are present on both the front and back sides of the hexagonal aluminum plate as shown in the orange part of the picture. The central star-shaped part with a length c of 13.27 mm and a width b of 6 mm is cut out, as indicated by the white color. The red dotted lines outline the unit cell with in-plane lattice constant of $a = 30\,mm$. When expressed using lattice vectors, the unit cell can be described as a_1 = (0, a) and a_2=(-a/2, $\sqrt{3}a/2$). As shown in Figure 1c, the thickness of the aluminum hexagonal thin plate and the height of the lead fan-shaped structure are $h_l = 1mm$ and $h_a = 5mm$, respectively. The elastic modulus of the aluminum hexagonal thin plate is $E = 73\ GPa$, with a density of ρ = 2,590 kg/m^3 and a Poisson's ratio of $\nu = 0.23$. The elastic modulus of Lead fan-shaped structure is $E = 16\ GPa$. The density and Poisson's ratio are ρ = 11340 kg/m^3 and ν = 0.42, respectively.

2.2 Theory

The propagation of elastic waves through the structure is governed (Huo et al., 2021):

$$\rho\ddot{\mathbf{u}} = \nabla(\lambda\nabla\mathbf{u}) + \nabla\left[\mu(\mathbf{u}\nabla + \nabla\mathbf{u})\right] \tag{1}$$

where ρ represents the material density and $\boldsymbol{u}$ is the displacement vector, λ and μ are lame constant.

The dynamic problem in periodic structures is addressed using Bloch-Floquet wave theory (Kittel and McEuen, 2018). The boundary condition can be expressed as in Equation 2:

$$\mathbf{u}(\mathbf{r},t) = \mathbf{u}_\mathbf{k}(\mathbf{r})e^{i(\mathbf{k}\cdot\mathbf{r}+\omega t)} \tag{2}$$

where $\boldsymbol{k}$ is the Bloch vector, r is spatial position, ω is the eigen frequency. Applying the Bloch-Floquet boundary condition, the dynamic problem in Equation 1 can be simplified to the following eigenvalue problem in Equation 3:

$$(\mathbf{K} - \omega^2\mathbf{M})\mathbf{u} = 0 \tag{3}$$

where the **M** and **K** represent the mass matrix and stiffness matrix of the model, respectively. Then, COMSOL Multiphysics is used to calculate the band structure by scanning the first Brillouin zone with respect to the wavevector $\boldsymbol{k}$, followed by the analysis of elastic wave propagation properties.

3 Valley-protected elastic wave properties

3.1 Dispersion analysis and band inversion

As depicted in Figure 2, the unit cell exhibits three distinct configurations, corresponding to those in Figure 2a the state with zero rotation angle, where the structure maintains symmetry; (b) the case with a positive rotation angle, indicating that the internal circular sector of the hexagon has undergone clockwise rotation relative to state (a); and (c) the case with a negative rotation angle, where the internal circular sector has rotated counterclockwise relative to state (a). Then, a parameter Δφ is defined to characterize the angular deviation relative to the symmetric configuration.

When $\Delta\varphi = 0$, the model simultaneously satisfies both time-reversal and spatial inversion symmetry. Subsequently, the band structure is calculated and presented in Figure 3a. It can be seen that the 4th and 5th branches degenerate at K point, which is known as Dirac degeneracy. To explore the topological properties of the model at this point, a perturbation with $\Delta\varphi = 1°$ is introduced to break the spatial symmetry of the unit cell. As shown in Figure 3b, after the symmetry is broken, the Dirac degeneracy is lifted and forming a bandgap.

To elucidate the topological properties of elastic waves, the band inversion process at the degenerate point is presented. Figure 4 visually depicts how the topological phase evolves as Δφ changes continuously. It can be distinctly observed that as $\Delta\varphi$ continuously increases, the bandgap first closes and then reopens.

The eigenstates of the two bands above and below the bandgap are denoted as ψ^+ and ψ^-, respectively, with the sign indicating the direction of the eigenmode. When $\Delta\varphi < 0$, eigenstates ψ^+ is located

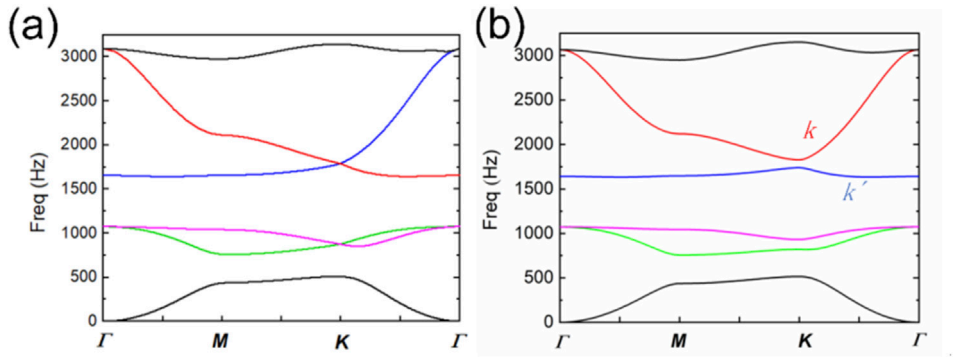

FIGURE 3
Band structure corresponds to the unit cell with **(a)** $\Delta\varphi = 0$ (solid lines) and **(b)** $\Delta\varphi \neq 0$.

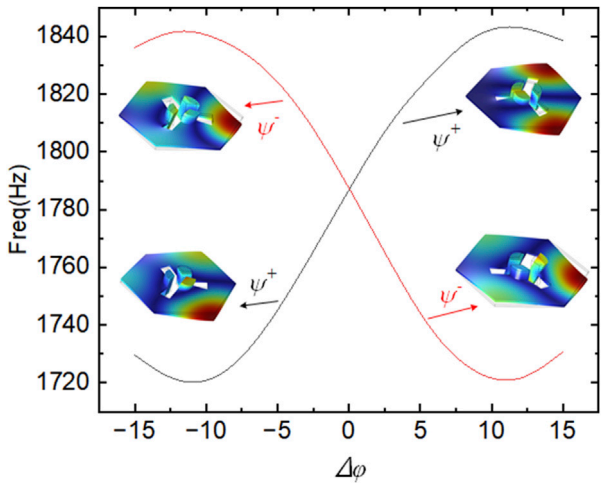

FIGURE 4
The phase transition at the K point under the continuous variation of $\Delta\varphi$.

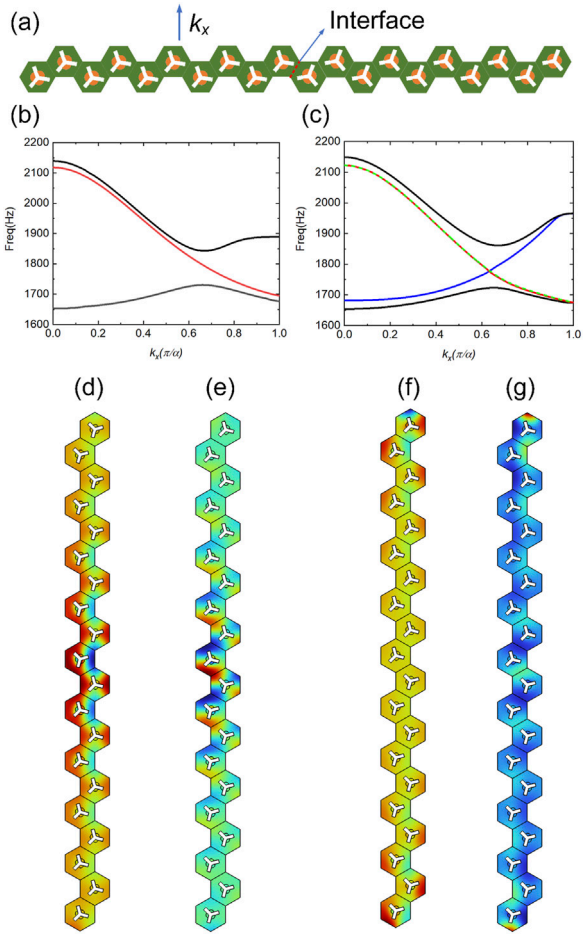

FIGURE 5
(a) Schematic diagram of the 1D supercell structure, the geometrical parameter on the two side of the interface is opposite; **(b,c)** Band structure of the model with perturbation parameter $\Delta\varphi = 15°$ and $\Delta\varphi = -15°$; **(d)** The modal displacement corresponds to the interface state represented by the red solid line in **(b)**; **(e)** The modal displacement corresponds to the interface state represented by the blue solid line in **(c)**; **(f,g)** the edge state corresponds to the green dashed line and red solid line in **(c)**.

above ψ^-, whereas for $\Delta\varphi > 0$, the positions are reversed. This indicates that a topological phase transition takes place when the symmetry is broken. Combined with the dispersion curves in Figure 3, we can infer that the breaking of symmetry leads to non-trivial topological states.

Based on the kp perturbation theory (Chen et al., 2018), when the system satisfies the condition of perturbation energy difference $\Delta E \neq 0$, it indicates that the equivalent model corresponds to a non-degenerate or weakly degenerate system obtained after perturbation treatment. For such perturbative treated systems, the effective Hamiltonian can be expressed as in Equations 4, 5:

$$\Delta\mathbf{H}\psi = \Delta\omega\psi \tag{4}$$

$$\Delta\mathbf{H} = v_D\delta k_x\boldsymbol{\sigma}_x + v_D\delta k_y\boldsymbol{\sigma}_y + mv_D^2\boldsymbol{\sigma}_z \tag{5}$$

where σ_x, σ_y and σ_z are the Pauli matrices, v_D is the Dirac velocity, $m = (\omega_{\psi^+} - \omega_{\psi^-})/2v_D^2$ is the Dirac mass. $\delta\boldsymbol{k}$ represents the deviation

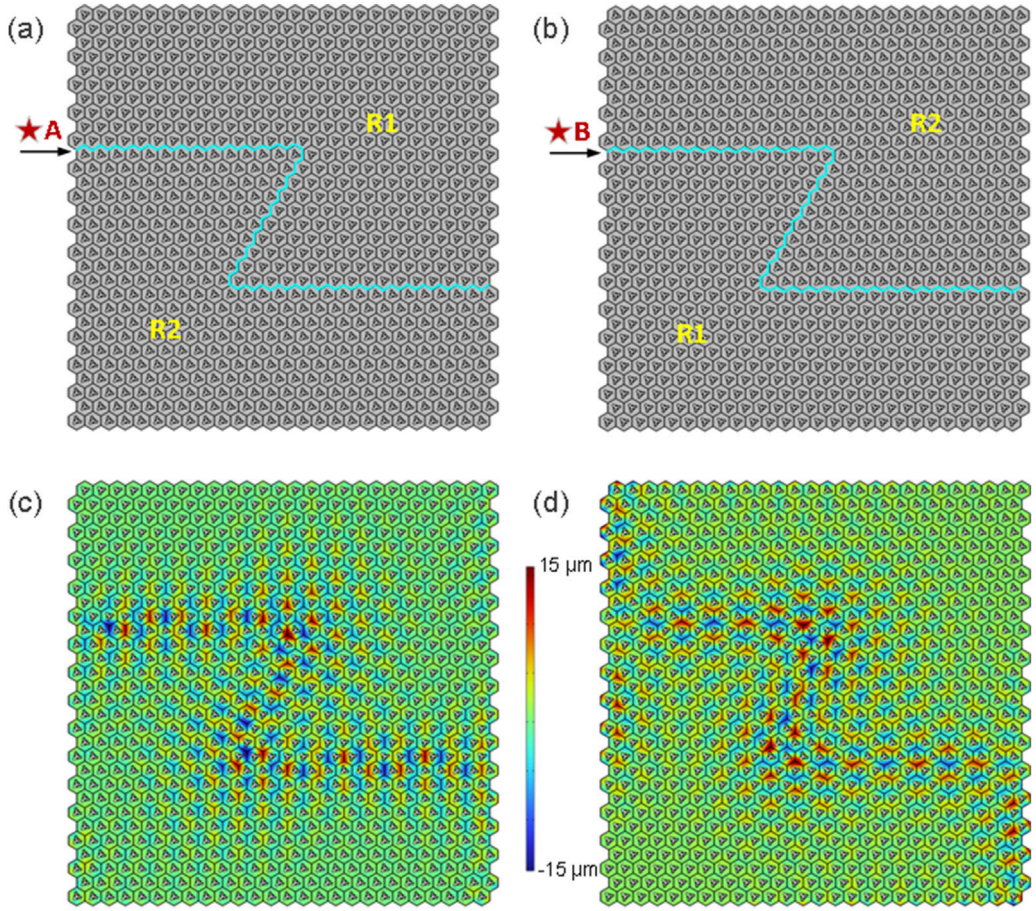

FIGURE 6
(a,b) Schematic of the Z-shaped interface path with different perturbation parameters; **(c,d)** Displacement field distribution of the model in **(a,b)** respectively.

from the Dirac point. The Berry curvature can be expressed as in Equation 6

$$\Omega(\delta\mathbf{k}) = \frac{1}{2} m v_D \left(\delta k^2 + m^2 v_D^2\right)^{-3/2} \tag{6}$$

The Valley Chern number is calculated in Equation 7

$$C_v = \frac{1}{2\pi} \int \Omega(\delta \boldsymbol{k}) dS \tag{7}$$

The Berry curvature plays a central role in the analysis of topological properties, with its physical significance lying in quantifying the local curvature of the wave-function in momentum space. This physical quantity serves as a key basis for determining topological invariants (such as the valley Chern number) and identifying topologically protected states, directly guiding the research direction of a system's topological properties. From the perspective of spatial distribution characteristics, the Berry curvature exhibits opposite signs in the upper and lower regions of the Brillouin zone (positive in the upper region and negative in the lower region). This feature provides the foundation for integration over partitioned regions. Taking the distribution corresponding to the blue line as seen in Figure 3b, integration over the upper and lower regions yields the numerical results $C_k = 0.5$ and $C_{k'} = -0.5$, respectively. Based on the definition of the valley Chern number, $C_v = C_k - C_{k'}$, the calculation gives a nonzero integer value of $C_v = 1$ According to the criterion for topological phase transitions, this result unambiguously confirms the occurrence of a valley-dependent topological phase transition in the system.

3.2 1D topological protected interface state analysis

To verify the existence of topologically protected interface states within the bandgap induced by symmetry breaking at the K point in this metamaterial, this study further investigates the dispersion characteristics of a supercell consisting of 20 unit cells. As illustrated in Figure 5, the interface is defined at the boundary between two types of structural units. The supercell model employs free boundary conditions at both ends, with Bloch periodic boundary conditions applied along the k_x as shown in Figure 5A.

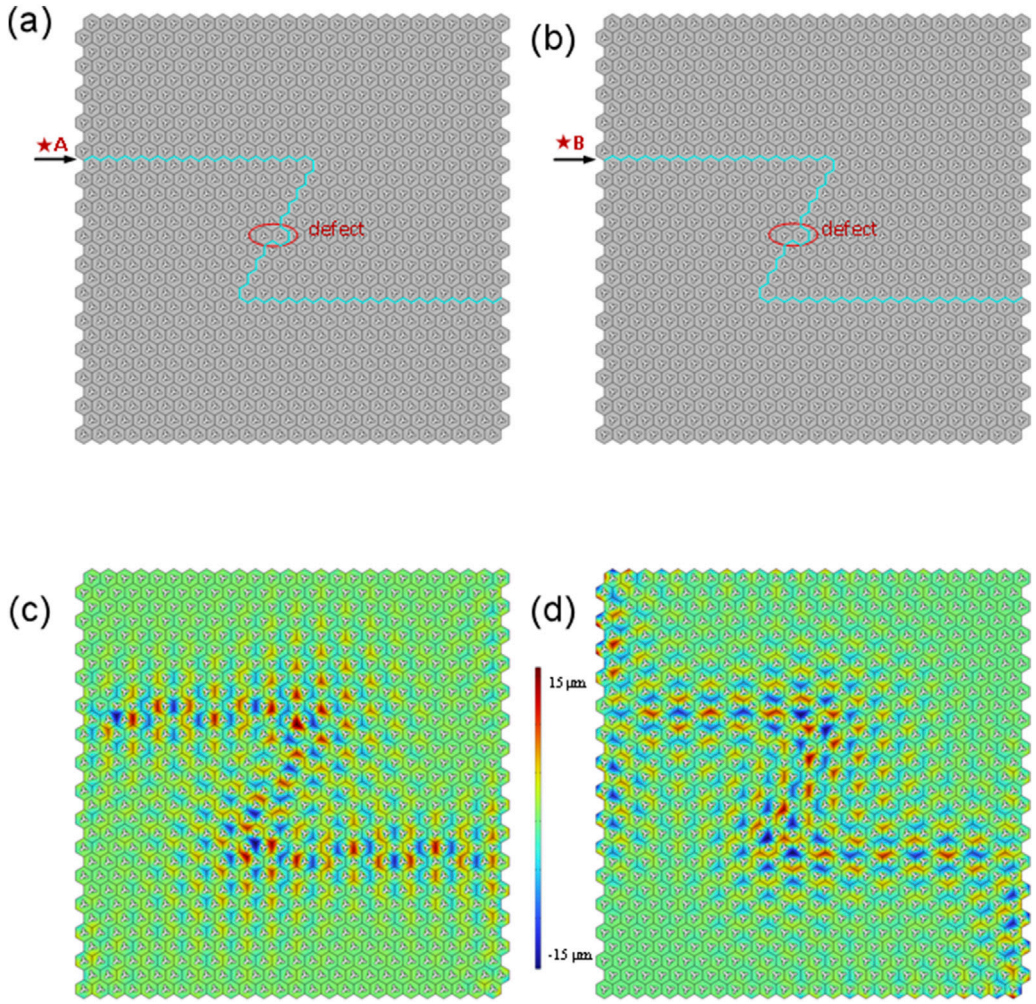

FIGURE 7
(a,b) Schematic of the Z-shaped interface path with bends local defects; **(c,d)** Displacement field distribution of the model in **(a,b)** respectively.

As shown in Figures 5b,c, the edge-bulk band structure of the 1D supercell correspond to $\Delta\varphi = 15°$ and $\Delta\varphi = -15°$, respectively, are calculated. As shown in Figure 5b, when $\Delta\varphi = 15°$, a dispersion branch associated with the interface state appears within the bandgap. Figure 5d illustrates the eigenmode on this dispersion branch at $f = 1797Hz$. The displacement distribution is concentrated near the interface. When $\Delta\varphi = -15°$, a dispersion branch related to the interface state, along with two dispersion branches associated with boundary states, appears within the bandgap, as illustrated by the blue solid line, red solid line and green dashed line in Figure 5c, respectively. Figure 5e shows the eigenmode corresponding the dashed line in Figure 5c at $f = 1779Hz$. The displacement distribution is localized near the interface. Figure 5f and (g) present the eigenmodes on the green dashed and red solid branches at $f = 1775Hz$ and $f = 1770Hz$, respectively. The modal displacement is primarily localized at the two ends of the 1D supercell. Obviously, the numerical simulation results show that the proposed model exhibits topological interface states, which can be realized by introducing a geometry perturbation with $\Delta\varphi \neq 0$.

3.3 2D topological protected local interface state

Figure 6 illustrates the numerical results of elastic wave propagation in the frequency domain for interfaces with distinct topological phases. As shown in Figures 6a,b, perturbation parameters for the models are $\Delta\varphi = 15°$. In both models, the interface path is configured in a Z-shape. The interface divides the model into two regions, R1 and R2. As is shown in Figure 5a, the perturbation parameters in R1 is $\Delta\varphi = -15°$ and the perturbation parameters in R2 is $\Delta\varphi = 15°$. The perturbation parameter distribution in Figure 6b is opposite. Figure 6c,d illustrate the frequency-domain displacement field corresponding to point excitations at locations A and B in Figures 6a,b, respectively. It can be observed that under point excitation, the interface state is confined to a localized region and does not propagate into the inner of region R1 and R2. It should be pointed out that the displacement on both sides in Figure 6d are caused by the edge state in Figures 5f,g. Then we set a local protrusion structure in the middle of the Z-shaped path, which can be equivalent to a local defect of the path. Figures 7c,d and Figure 8 show the displacement field distribution

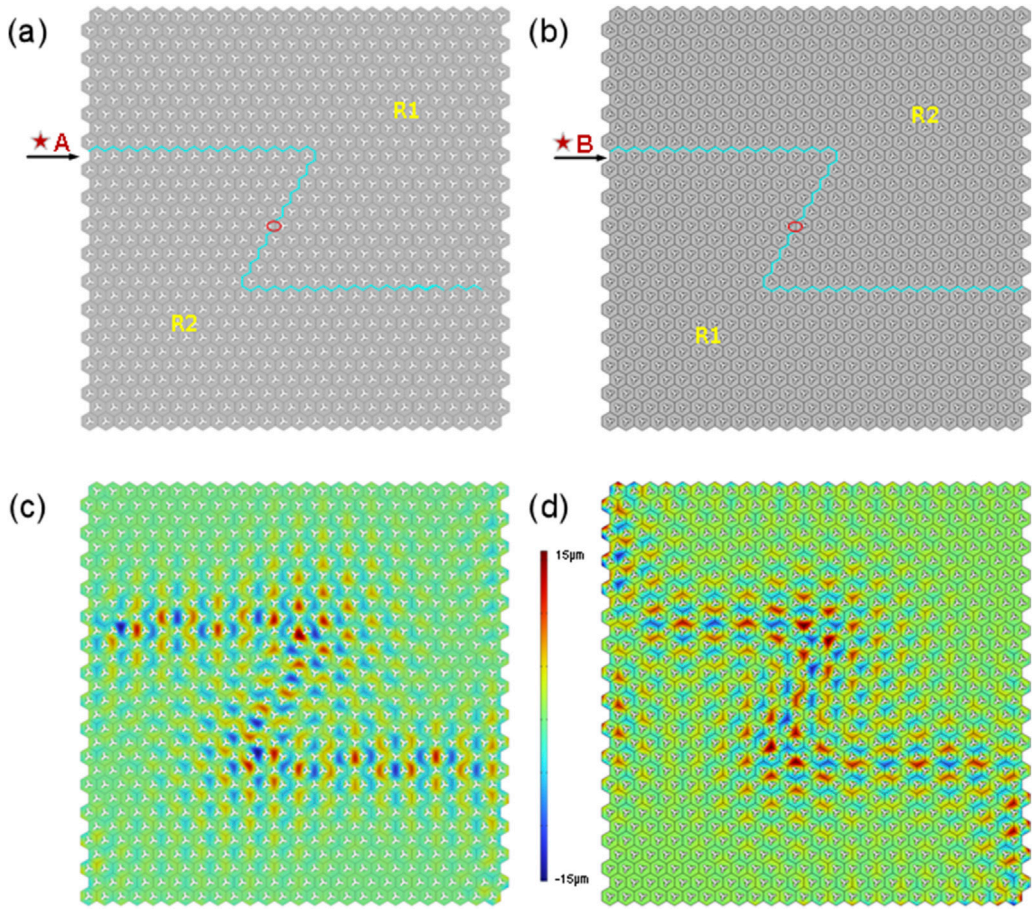

FIGURE 8
(a,b) Schematic of the Z-shaped interface path with local defects of discontinuous angles; **(c,d)** Displacement field distribution of the model in **(a,b)** respectively.

after introducing this local defect. The amplitude of the point excitation is 15 μm, and as can be seen from the figure, the vibration amplitude remains approximately 15 μm along the entire path up to the end. It can be can be concluded that the topologically protected interface states exhibit significant robustness against the defect—elastic waves can still penetrate the defect and propagate continuously.

4 Conclusion

This paper presents a topological metamaterial design based on the introduction of geometrical rotation parameter, which subsequently breaks the spatial inversion symmetry. The topological band inversion can be realized by continuously changing the geometrical rotation parameter $\Delta\varphi$. The physical mechanism of the topological phase transition is characterized by the kp perturbation theory. Both the theoretical and numerical analysis indicate that the introduction of a geometrical rotation can break the spatial reversion symmetry, thereby facilitating the design of a topologically nontrivial state. Also, the interface state characteristics of the metamaterial within the Dirac bandgap are investigated through numerical simulation. The interface states of the metamaterial are localized in a small region near the interface and can propagate along the interface. This localized characteristic enables the realization of complex local vibration patterns within the plane.

Data availability statement

The original contributions presented in the study are included in the article/supplementary material, further inquiries can be directed to the corresponding author.

Author contributions

YW: Writing – original draft. SY: Data curation, Writing – original draft. CJ: Software, Writing – review and editing. JH: Validation, Writing – review and editing.

Funding

The author(s) declared that financial support was received for this work and/or its publication. This work was funded by Jiangsu Provincial Qinglan Engineering Project for Higher Education

Institutions (Grant No. 2023QL003) and Major Projects of Basic Science (Natural Science) Research in Colleges and Universities of Jiangsu Province (Grant No. 22KJA460008).

Conflict of interest

The author(s) declared that this work was conducted in the absence of any commercial or financial relationships that could be construed as a potential conflict of interest.

Generative AI statement

The author(s) declared that generative AI was not used in the creation of this manuscript.

Any alternative text (alt text) provided alongside figures in this article has been generated by Frontiers with the support of artificial intelligence and reasonable efforts have been made to ensure accuracy, including review by the authors wherever possible. If you identify any issues, please contact us.

Publisher's note

All claims expressed in this article are solely those of the authors and do not necessarily represent those of their affiliated organizations, or those of the publisher, the editors and the reviewers. Any product that may be evaluated in this article, or claim that may be made by its manufacturer, is not guaranteed or endorsed by the publisher.

References

Abadal, S., Cui, T., Low, T., and Georgiou, J. (2020). Programmable metamaterials for software-defined electromagnetic control: circuits, systems, and architectures. *IEEE J. Emerg. Sel. Top. Circuits Syst.* 10, 6–19. doi:10.1109/jetcas.2020.2976165

Akbari-Farahani, F., and Ebrahimi-Nejad, S. (2024). From defect mode to topological metamaterials: a state-of-the-art review of phononic crystals and acoustic metamaterials for energy harvesting. *Sensors Actuators A Phys.* 365. doi:10.1016/j.sna.2023.114871

Bernevig, B. A., and Zhang, S. C. (2006). Quantum spin hall effect. *Phys. Rev. Lett.* 96, 106802. doi:10.1103/PhysRevLett.96.106802

Cao, L., Zhu, Y., Wan, S., Zheng, Y., and Assouar, B. (2022). On the design of Non-Hermitian elastic metamaterial for broadband perfect absorbers. *Int. J. Eng. Sci.* 181, 103768. doi:10.1016/j.ijengsci.2022.103768

Cao, J., Qi, F., and Yan, S. (2025). The required acoustic parameters simplification of invisibility cloaks and concentrators using the impedance-tunable coordinate transformation. *Sci. Rep.* 11, 920. doi:10.1038/s41598-020-79728-7

Chen, H., Nassar, H., Norris, A. N., Hu, G. K., and Huang, G. L. (2018). Elastic quantum spin hall effect in kagome lattices. *Phys. Rev. B* 98, 094302. doi:10.1103/physrevb.98.094302

Chen, Y., Liu, D., Wu, Y., Yu, P., and Liu, Y. (2023). Valley hall elastic topological insulator with large chern numbers. *Int. J. Mech. Sci.* 239, 107884. doi:10.1016/j.ijmecsci.2022.107884

Chen, Y., Guo, Z., Liu, Y., Li, J., and Yu, Z. (2024a). Rainbow trapping and concentration of surface waves on broad waveguide. *J. Phys. D. Appl. Phys. A Europhys. J.* (46), 57.

Chen, Y., Liu, Y., Huang, J., Li, J., and Yan, L. (2024b). Elastic topological resonator in pseudo-spin hall edge states. *Mech. Adv. Mater. Struct.* 31 (26), 7801–7811. doi:10.1080/15376494.2023.2250368

Chen, Y., Fan, L., Zhu, J., and Su, Z. (2024c). An all-polarized elastic topological metamaterial for ultrasonic energy conveying and harvesting. *Adv. Funct. Mater.* 35, 2413285. doi:10.1002/adfm.202413285

Chen, C., Zhang, Y., Zheng, Y., Zhang, Y., Liu, H., Wu, J., et al. (2025a). Topology in biological piezoelectric materials. *Adv. Mater* 37, e2500466. doi:10.1002/adma.202500466

Chen, Y., Yan, L., Lei, B., Yu, Z., and Liu, Y. (2025b). Topological dislocation in quadrupole square lattice with nonsymmorphic symmetries. *Appl. Acoust.* 239, 110827. doi:10.1016/j.apacoust.2025.110827

Chen, Y., Lei, B., Wu, Y., Liu, Y., and Yu, Z. (2025c). Elastic dislocation states of full-polarization micromechanical metamaterials. *Thin-Walled Struct.* 214, 113270. doi:10.1016/j.tws.2025.113270

Chu, Y., Sun, T., Wang, Z., and Zhang, Z. (2024). Dual-band topological refractive properties in solid phononic crystals. *Phys. Lett. A* 525, 129881. doi:10.1016/j.physleta.2024.129881

Darabi, A., Ni, X., Leamy, M., and Alu, A. (2020). Reconfigurable floquet elastodynamic topological insulator based on synthetic angular momentum bias. *Sci. Adv.* 6, eaba8656. doi:10.1126/sciadv.aba8656

Den, N. M. (1982). Quantized hall conductance in a two-dimensional periodic potential. *Phys. A Stat. Mech. and Its Appl.* 124.

Dong, X., Chen, K., Zhang, J., and Peng, Z. (2024). Topological valley mode separation of elastic waves and potential applications. *Int. J. Mech. Sci.* 274, 109229. doi:10.1016/j.ijmecsci.2024.109229

Du, C., Ning, L., Ma, T., and Liu, J. (2025). Manipulation of flexural waves in reconfigurable piezoelectric metamaterial resonator lattices. *Phys. Scr.* 100, 085935. doi:10.1088/1402-4896/adf2fb

Haldane, F. D. M. (1988). Model for a quantum hall effect without landau levels: condensed-matter realization of the parity anomaly. *Phys. Rev. Lett.* 61 (18), 2015–2018. doi:10.1103/PhysRevLett.61.2015

Huo, S., Chen, J., Huang, H., Wei, Y., Tan, Z., Feng, L., et al. (2021). Experimental demonstration of valley-protected backscattering suppression and interlayer topological transport for elastic wave in three-dimensional phononic crystals. *Mech. Syst. Signal Process* 154, 107543. doi:10.1016/j.ymssp.2020.107543

Jia, Q., Zhang, J., Han, D., Wen, J., and Yu, D. (2025). Bragg scattering-driven anisotropic metabeam with multi-scale architecture for ultra-broadband vibration suppression at high structural stiffness. *Eng. Struct.* 336, 120493. doi:10.1016/j.engstruct.2025.120493

Jiao, P., Mueller, J., Raney, J. R., Zheng, X. R., and Alavi, A. H. (2023). Mechanical metamaterials and beyond. *Nat. Commun.* 14, 6004. doi:10.1038/s41467-023-41679-8

Kittel, C., and McEuen, P. (2018). *Introduction to solid state physics*. John Wiley and Sons.

Klitzing, K. V., Dorda, G., and Pepper, M. (1980). New method for high-accuracy determination of the fine-structure constant based on quantized hall resistance. *Phys. Rev. Lett.* 45 (6), 494–497. doi:10.1103/physrevlett.45.494

Li, S., Kim, I., Iwamoto, S., Zang, J., and Yang, J. (2019). Valley anisotropy in elastic metamaterials. *Phys. Rev. B* 100, 195102. doi:10.1103/physrevb.100.195102

Li, X., Yu, S., Liu, H., Lu, M., and Chen, Y. (2020). Topological mechanical metamaterials: a brief review. *Curr. Opin. Solid State Mater. Sci.* 24, 100853. doi:10.1016/j.cossms.2020.100853

Liu, J., Ma, Z., Gao, J., and Dai, X. (2019). Quantum valley hall effect, orbital magnetism, and anomalous hall effect in twisted multilayer graphene systems. *Phys. Rev. X* 9, 031021. doi:10.1103/physrevx.9.031021

Lu, J., Qiu, C., Ye, L., Fan, X., Ke, M., Zhang, F., et al. (2016). Observation of topological valley transport of sound in sonic crystals. *Nat. Phys.* 13, 13369–13374. doi:10.1038/nphys3999

Mousavi, S. H., Khanikaev, A. B., and Wang, Z. (2015). Topologically protected elastic waves in phononic metamaterials. *Nat. Commun.* 6, 8682. doi:10.1038/ncomms9682

Nash, L. M., Kleckner, D., Read, A., Vitelli, V., Turner, A. M., and Irvine, W. T. (2015). Topological mechanics of gyroscopic metamaterials. *Proc. Natl. Acad. Sci. U. S. A.* 112, 14495–14500. doi:10.1073/pnas.1507413112

Ni, A., and Shi, Z. (2023). Robust elastic wave transport in zone-folding induced topological hierarchical metamaterials. *Int. J. Mech. Sci.* 251, 108336. doi:10.1016/j.ijmecsci.2023.108336

Ni, X., Yves, S., Krasnok, A., and Alu, A. (2023). Topological metamaterials. *Chem. Rev.* 123, 7585–7654. doi:10.1021/acs.chemrev.2c00800

On, M. B., Ashtiani, F., Sanchez-Jacome, D., Perez-Lopez, D., and Yoo, S. J. B. (2024). A blanco-redondo, programmable integrated photonics for topological hamiltonians. *Nat. Commun.* 15, 629. doi:10.1038/s41467-024-44939-3

Pendry, J. B., Schurig, D., and Smith, D. R. (2006). Controlling electromagnetic fields. *Science* 312, 1780–1782. doi:10.1126/science.1125907

Qi, D., Ren, Z., and Qu, Z. (2022). Valley-protected topological interface state of the elastic wave: from discrete model to multistable mechanical metamaterials. *J. Sound Vib.* 529, 116908. doi:10.1016/j.jsv.2022.116908

Rao, Z., Meng, C., Han, Y., Zhu, L., Ding, K., and An, Z. (2024). Braiding reflectionless states in Non-Hermitian magnonics. *Nat. Phys.* 20 (12), 1904–1911. doi:10.1038/s41567-024-02667-x

Santoro, R., Mazzeo, M., and Failla, G. (2023). A computational framework for uncertain locally resonant metamaterial structures. *Mech. Syst. Signal Process* 190, 110094. doi:10.1016/j.ymssp.2023.110094

Susstrunk, R., and Huber, S. D. (2015). Observation of phononic helical edge states in a mechanical topological insulator. *Science* 349, 47–50. doi:10.1126/science.aab0239

Wang, G., Wan, S., Li, D., Li, L., Liu, S., and Li, X. (2025). Chatter suppression for milling based on local resonance elastic metamaterials. *J. Manuf. Process.* 146, 359–379. doi:10.1016/j.jmapro.2025.04.102

Xiu, H., Liu, H., Poli, A., Wan, G., Sun, K., Arruda, E. M., et al. (2022). Topological transformability and reprogrammability of multistable mechanical metamaterials. *Proc. Natl. Acad. Sci. U. S. A.* 119, e2211725119. doi:10.1073/pnas.2211725119

Yi, J., Long, J., and Chen, C. (2023). Reconfigurable higher-order topological electromechanical metamaterial. *Extreme Mech. Lett.* 65, 102105. doi:10.1016/j.eml.2023.102105

Zhang, Z., Wei, Q., Cheng, Y., Zhang, T., Wu, D., and Liu, X. (2017). Topological creation of Acoustic pseudospin multipoles in a flow-free symmetry-broken metamaterial lattice. *Phys. Rev. Lett.* 118, 084303. doi:10.1103/PhysRevLett.118.084303

Zhang, Q., Chen, Y., Zhang, K., and Hu, G. (2019). Programmable elastic valley hall insulator with tunable interface propagation routes. *Extreme Mech. Lett.* 28, 76–80. doi:10.1016/j.eml.2019.03.002

Zhang, K., Hong, F., Luo, J., and Deng, Z. (2022). Topological edge state analysis of hexagonal phononic crystals. *Acta Mech. Sin.* 38, 421455. doi:10.1007/s10409-021-09030-x